Water column iron dynamics in the subarctic North Pacific Ocean and the Bering Sea

Ren Uchida,[1] Kenshi Kuma,[1,2] Aya Omata,[1] Satoko Ishikawa,[1] Nanako Hioki,[2] Hiromichi Ueno,[1,2] Yutaka Isoda,[2] Keiichiro Sakaoka,[2] Yoshihiko Kamei,[2] and Shohgo Takagi[2]

Received 10 August 2012; revised 19 January 2013; accepted 23 January 2013; published 18 March 2013.

[1] We measured water-column iron concentrations from west to east along 47°N in the subarctic North Pacific, and in the Bering Sea. In the North Pacific dissolved Fe (D-Fe) showed surface depletion, mid-depth maxima at 1000–1500 m (west, 1.3–1.6 nM; east, 0.9–1.1 nM), and a gradual decrease with depth below 3500–4000 m depth (west, 1.1–1.4 nM; east, 0.6–0.7 nM). D-Fe and total soluble Fe (T-Fe) in deep water showed a decreasing trend eastward. The higher iron concentrations in western deep waters probably result from higher inputs of dissolved Fe through atmospheric deposition or lateral transport. In contrast, D-Fe throughout the Bering Sea showed a consistent depth regime characterized by a rapid increase with depth to mid-depths, a gradual increase with depth in intermediate water to a maximum of 1.6–1.7 nM at 1500–2250 m, and a gradual decrease with depth to 1.3–1.4 nM at 3700 m. Higher iron concentrations and deeper D-Fe maxima in the Bering Sea are likely due to higher biological productivity and greater and deeper D-Fe input from the decomposition of sinking particulate organic matter in deep water. We suggest that the higher concentrations and deeper input of D-Fe as well as PO_4 and humic-type fluorescent dissolved organic matter in the Bering Sea probably results from the longer time for the accumulation of decomposition products resulting from iron supply from the organic-rich downslope sediment along the steep continental slopes and slow replacement of the deep water in the Bering Sea Basin.

Citation: Uchida, R., K. Kuma, A. Omata, S. Ishikawa, N. Hioki, H. Ueno, Y. Isoda, K. Sakaoka, Y. Kamei, and S. Takagi (2013), Water column iron dynamics in the subarctic North Pacific Ocean and the Bering Sea, *J. Geophys. Res. Oceans*, *118*, 1257–1271, doi:10.1002/jgrc.20097.

1. Introduction

[2] Many studies of iron in the North Pacific Ocean show vertical distributions of iron concentrations that have nutrient-like profiles, characterized by surface depletion due to biological uptake and mid-depth maxima due to remineralization of iron-rich biological matter [*Martin et al*., 1989; *Bruland et al*., 1994; *Nakabayashi et al*., 2001; *Nishioka et al*., 2003, 2007]. However, several recent studies of iron distributions revealed that dissolved iron (D-Fe) concentrations in deep waters of the western North Pacific [*Nakabayashi et al*., 2001; *Takata et al*., 2006; *Nishioka et al*., 2003, 2007; *Kitayama et al*., 2009] are approximately double those in the eastern and central North Pacific [*Martin et al*., 1989; *Bruland et al*., 1994; *Nishioka et al*., 2003; *Takata et al*., 2006; *Kitayama et al*., 2009]. These differences reflect regional patterns of eolian source, physical transport, and the water column processes involved in the cycling of iron, such as biological uptake, remineralization of biogenic matter, scavenging onto particles, and iron complexation with natural organic ligands [*Kuma et al*., 1996; *Johnson et al*., 1997a, 1997b]. It has recently been suggested that Fe(III) hydroxide solubility in deep water is controlled by organic Fe(III) complexation with humic-type fluorescent dissolved organic matter (humic-type FDOM), which plays an important role in regulating D-Fe in the deep water column [*Tani et al*., 2003; *Kitayama et al*., 2009; *Yamashita et al*., 2010; *Nakayama et al*., 2011]. The Bering Sea is one of the largest marginal seas for which our understanding of the biogeochemical and physical mechanisms that regulate iron and other trace metals is still limited. There have been only a few studies on iron distributions in the Bering Sea Basin [*Fujishima et al*., 2001; *Takata et al*., 2005; *Aguilar-Islas et al*., 2007; *Hurst et al*., 2010], the Okhotsk Sea Basin [*Tani et al*., 2003; *Nishioka et al*., 2007], and the Japan Sea Basin [*Takata et al*., 2005, 2008; *Fujita et al*., 2010]. The surface circulation in the Bering Sea is a cyclonic gyre, with the southward flowing Kamchatka Current forming the western

[1]Graduate School of Environmental Science, Hokkaido University, Sapporo, Kita 10-Nishi 5, Kita-ku, Sapporo, Hokkaido, Japan.
[2]Faculty of Fisheries Sciences, Hokkaido University, Hokkaido, Japan.

Corresponding author: K. Kuma, Faculty of Fisheries Sciences, Hokkaido University, 3-1-1 Minato, Hakodate, Hokkaido 041-8611, Japan. (kuma@fish.hokudai.ac.jp)

2169-9275/13/10.1002/jgrc.20097

boundary current and northward flowing Bering Slope Current. The Kamchatka Current flows southward until it splits, with a portion entering the Sea of Okhotsk and the rest continuing along the Kuril Islands to join the Oyashio. The oceanic portion of the Bering Sea basin is influenced by Alaskan Stream water that enters the Bering Sea through the many passes in the Aleutian Island arc: Near Strait (sill depth approximately 2000 m), Buldir Pass (sill depth 640 m), Amchitka Pass (sill depth 1155 m) and Amukta Pass (sill depth 430 m) (Figure 1). These passes allow Alaskan Stream water to join with the Aleutian North Slope Current (ANSC) along the northern side of the Aleutian Islands [*Reed and Stabeno*, 1990, *Stabeno et al*., 1999].

[3] The northward transport into the Bering Sea, along with the flow through Near Strait and Amchitka Pass, is the source of the ANSC and ultimately the Bering Slope Current (BSC) [*Reed and Stabeno*, 1999]. Most of the transport into the Bering Sea occurs through Near Strait. The inflow into the Bering Sea is balanced by outflow through the Kamchatka Strait (sill depth approximately 4000 m) [*Stabeno et al*., 1999]. The Kamchatka Strait is not only the location of the majority of Bering Sea outflow but also the only gateway into the Bering Sea that is deep enough (>2000 m) to permit inflow of Deep Pacific Water. Vertical sections of temperature, salinity, sigma-*t*, and $Si(OH)_4$ across the Kamchatka Strait indicate the inflow of deep water below 2500 m on the eastern side of the strait and a return flow of upper deep water (near 2500 m) on the western side of the strait [*Reed et al*., 1993]. The path of deep water is northeastward from the Kamchatka Strait with some return flow above 3000 m on the western side.

[4] Deep water in the Bering Sea Basin is warmer, less salty, less oxygenated, and has higher concentrations of $Si(OH)_4$ than that in the North Pacific Ocean [*Tsunogai et al*., 1979; *Roden*, 1995, 2000]. The bottom water slowly displaces the deep water above. At the same time, $Si(OH)_4$ concentrations are increased by regeneration both within the water columns and from the bottom. Model results suggest that regeneration of $Si(OH)_4$ from bottom sediments is much more important than that taking place in the water column, and that bottom regeneration rates are approximately four to five times those within the water columns [*Coachman et al*., 1999]. This is in agreement with the results of *Tsunogai et al*. [1979], who reported that bottom $Si(OH)_4$ regeneration in the Bering Sea is four to five times that occurring in the deep water of the North Pacific. In addition, both *Tsunogai et al*. [1979] and *Coachman et al*. [1999] estimated seawater residence times of approximately 300–400 years for the deep Bering Sea.

[5] In the present study, we compared the vertical distributions of D-Fe, total soluble Fe (T-Fe), and chemical components (nutrients, apparent oxygen utilization [AOU], and humic-type FDOM) in the deep waters of the subarctic North Pacific Ocean and the Bering Sea. Our goal was to determine the factors controlling the vertical distribution of iron on the basis of deep water circulation in the subarctic North Pacific Ocean and the semiclosed marginal Bering Sea, and the water exchange between them.

2. Materials and Methods

2.1. Sample Collection and Treatment

[6] Samples were collected in the subarctic North Pacific Ocean (stations NP1–NP4 along a west-east line at 47°N

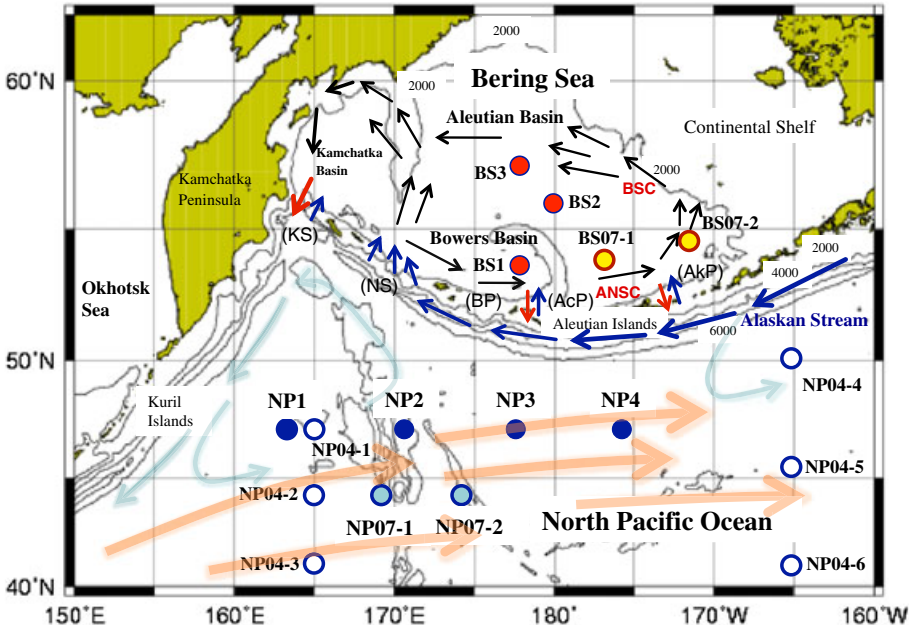

Figure 1. Sampling locations in the subarctic North Pacific and the Bering Sea Basin during 7 June–1 July 2009 and 7–20 July 2007. North Pacific stations: NP1–NP4 along 47°N latitude in 2009, NP07-1 and NP07-2 along 44°N latitude in 2007; Bering Sea stations: BS1 in Bowers Basin and BS2 and BS3 in the central Aleutian Basin in 2009; BS07-1 and BS07-2 in the southeastern Aleutian Basin in 2007. Solid circles, this study; open circles, previous studies along 165°E and 165°W longitude [*Takata et al*., 2005, 2006; *Kitayama et al*., 2009] (Table 1). AcP, Amchitka Pass; AkP, Amukta Pass; ANSC, Aleutian North Slope Current; BP, Buldir Pass; BSC, Bering Slope Current; KS, Kamchatka Strait; NS, Near Strait.

latitude) and the Bering Sea (station BS1 in Bowers Basin and stations BS2 and BS3 in the central Aleutian Basin) during 7 June–1 July 2009 (Figure 1 and Table 1). Samples were collected using acid-cleaned, Teflon-coated, 5-L Niskin X sampling bottles (General Oceanics) attached to a rosette multisampler along with a conductivity-temperature-depth (CTD) probe (SBE 19plus, Sea-Bird Electronics, Inc.). Samples were gravity filtered on deck for analysis of D-Fe by connecting an acid-cleaned 0.22 μm pore size membrane filter (Durapore cartridge type, Millipak 100; Millipore) to a sampling spigot on the Niskin bottles. Filtered samples for humic-type FDOM analysis were collected at stations NP07-1 and NP07-2 (near station NP2) in the subarctic North Pacific, and at BS07-1 and BS07-2 in the southeastern Bering Sea, during 7–20 July 2007 (Figure 1 and Table 1). The samples (7—8 ml) in 10-ml acrylic tubes (Sanplatec Corp.) were immediately frozen and kept below −20°C in the dark (1–2 months) until measurement in the laboratory. The earlier works [*Tani et al*., 2003; *Takata et al*., 2004, 2005, *Kitayama et al*., 2009] used low-density polyethylene (LDPE) bottles instead of acrylic tubes in the present study. Unfiltered samples were collected for T-Fe, Chl *a*, and nutrient concentrations. The filtered (<0.22 μm) and unfiltered seawater samples (100 ml) used for D-Fe and T-Fe analyses, respectively, were initially collected in precleaned 125-ml LDPE bottles, which were then acidified with ultrapure grade HCl to pH 1.7–1.8 in a class 100 clean air bench in a clean room on board after collection and then allowed to stand at room temperature for at least 3 months until iron analysis in the laboratory [*Bruland and Rue*, 2001]. Sample treatment in the present study was the same as in our previous studies [*Fujita et al*., 2010; *Nakayama et al*., 2011; *Nishimura et al*., 2012]. Hydrographic observations (salinity, temperature and depth) were conducted using a CTD.

2.2. Dissolved and Total Soluble Fe

[7] Acidified iron samples were buffered at pH 3.2 with a buffer solution of 8.15 M quartz-distilled formic acid and 4.54 M ultrapure grade ammonium (0.8 ml per 100-ml sample solution) in a class 100 clean-air bench in the laboratory on shore. The iron concentrations (D-Fe and T-Fe) in buffered 0.22-μm-filtered and unfiltered samples were determined by an automated Fe analyzer (Kimoto Electric Co. Ltd.) using a combination of chelating resin concentration and luminol-hydrogen peroxide chemiluminescence (CL) detection in a closed flow-through system [*Obata et al*., 1993] as described in our previous studies [*Nakabayashi et al*., 2001; *Takata et al*., 2004, 2006, 2008; *Kitayama et al*., 2009; *Fujita et al*., 2010; *Nakayama et al*., 2011; *Nishimura et al*., 2012]. Briefly, iron in a buffered sample was selectively collected on 8-hydroxyquinoline immobilized chelating resin and then eluted with dilute (0.3 M) HCl. The eluent was mixed successively with luminol solution, 0.6 M aqueous ammonia and 0.7 M H_2O_2, and then the mixture was introduced into the CL cell. Finally, the iron concentration was determined from the CL intensity. The accuracy of this analysis was checked using Sampling and Analysis of Fe (SAFe) reference materials (pH 1.7–1.8). The D-Fe in the SAFe surface (S) water and deep (D1) intercalibration waters, as determined by our analytical method in the present study after being buffered at pH 3.2, were 0.10 ± 0.01 nM (n = 6) for S and 0.70 ± 0.03 nM (n = 5) for D1, consistent with the community consensus values of 0.090 ± 0.007 nM for S and 0.67 ± 0.07 nM for D1 [*Johnson*, 2007; GEOTRACES {www.geotraces.org}].

Table 1. Locations of Sampling Stations in the Subarctic North Pacific and the Bering Sea, Including Bottom Depth, Sampling Date, and Parameters Measured

Position					
Station	Latitude (N)	Longitude (E or W)	Bottom Depth (m)	Sampling Date	Measured Parameters
(Subarctic North Pacific Ocean)					
NP1	47°00′	163°30′E	5745	7 Jun 2009	Fe, nutrient, oxygen (this study)
NP2	47°00′	170°29′E	6310	9 Jun 2009	Fe, nutrient, oxygen (this study)
NP3	47°00′	177°30′E	5478	11 Jun 2009	Fe, nutrient, oxygen (this study)
NP4	46°58′	175°30′W	5644	12 Jun 2009	Fe, nutrient, oxygen (this study)
NP07-1	44°00′	169°00′E	5553	7 Jul 2007	Humic F-intensity, oxygen (this study)
NP07-2	44°00′	174°00′E	5650	10 Jul 2007	Humic F-intensity, oxygen (this study)
NP04-1	47°00′	165°00′E	5884	Jul 2004, 3 Jul 2005	Humic F-intensity, Fe, nutrient, oxygen [*Takata et al*., 2006; *Kitayama et al*., 2009]
NP04-2	44°00′	165°00′E		Jul 2004	Fe, nutrient, oxygen [Takata et al., 2006]
NP04-3	41°00′	165°00′E		Jul 2004	Fe, nutrient, oxygen [Takata et al., 2006]
NP04-4	50°00′	165°00′W		Jul 2004	Fe, nutrient, oxygen [Takata et al., 2006]
NP04-5	45°30′	165°00′W		Jul 2004	Fe, nutrient, oxygen [Takata et al., 2006]
NP04-6	41°00′	165°00′W	5717	Jul 2004, 29–30 Jul 2005	Humic F-intensity, Fe, Nutrient, Oxygen [*Takata et al*., 2006; *Kitayama et al*., 2009]
(Bering Sea Basin)					
BS1	53°31′	178°01′E	3900	29 Jun 2009	Fe, nutrient, oxygen (this study)
BS2	55°59′	180°00′W	3840	30 Jun 2009	Fe, nutrient, oxygen (this study)
BS3	57°00′	178°00′E	3840	1 Jul 2009	Fe, nutrient, oxygen (this study)
BS07-1	53°22′	177°00′W	3778	03 Jul, 13 Jul 2007	Humic F-intensity, Fe, nutrient, oxygen [*Takata et al*., 2005] (this study)
BS07-2	54°00′	172°00′W	3261	20 Jul 2007	Humic F-intensity, oxygen (this study)

2.3. Nutrient, Chl *a*, Oxygen, and Humic-Type FDOM

[8] Major nutrient ($NO_3 + NO_2$, PO_4, and $Si(OH)_4$) concentrations were determined using an autoanalyzer (Technicon) using CSK standard solutions for nitrate and nitrite (Wako Pure Chemical Industries, Ltd., Japan) and standard methods [*Parsons et al.*, 1984]. The concentrations of Chl *a* were determined by fluorometry with a Turner Design fluorometer (model 10-AU-005) after extraction with N, N-dimethylformamide [*Suzuki and Ishimaru*, 1990]. Dissolved oxygen was determined on board by the Winkler titration method with potentiometric end-point using a 798 MPT Titrino analyzer (Metrohm). Apparent oxygen utilization (AOU) was calculated by subtracting the measured oxygen content from the dissolved oxygen saturation [*Hansen*, 1999].

[9] Humic-type FDOM was quantified by humic-type fluorescence intensity (humic F-intensity) as reported in our previous studies [*Tani et al.*, 2003; *Takata et al.*, 2004, 2005; *Kitayama et al.*, 2009; *Fujita et al.*, 2010]. The frozen 0.22 μm filtered samples in acrylic tubes were thawed and warmed overnight to room temperature in the dark, and then the humic F-intensity was measured in a 1-cm quartz cell by using an Hitachi F-2000 fluorescence spectrophotometer at 320 nm excitation (Ex) and 420 nm emission (Em) with 10-nm bandwidths [*Hayase et al.*, 1988; *Hayase and Shinozuka*, 1995]. Fluorescence intensity was expressed in terms of quinine sulfate units (1 QSU = 1 ppb quinine sulfate in 0.05 M H_2SO_4, excitation 320 nm, emission 420 nm; *Mopper and Schultz* [1993]) and then converted to the unified scale of fluorescence Raman units at an excitation wavelength of 350 nm (RU_{350}) by the equation $RU_{350} = QSU_{320/420} \times 0.012$ [*Lawaetz and Stedmon*, 2009; *Heller et al.*, 2012]. The vertical distributions and levels of humic F-intensity in the subarctic North Pacific in the present study were very similar to those in the northern North Pacific in the previous study [*Kitayama et al.*, 2009], which were measured after thawing the frozen 0.22 μm filtered samples in precleaned LDPE bottles.

3. Results

3.1. Physical Characteristics of the Subarctic North Pacific and the Bering Sea Water Column

[10] In the surface mixed layer (<20–40 m depth), the depth of which was estimated using temperature and density data, potential temperatures and salinities at stations NP1–NP4 in the subarctic North Pacific (6–10°C and 32.7–33.3, respectively) were similar to those at stations BS1–BS3 in the Bering Sea (6–7°C and 33.1–33.2; Figure 2). However, the surface salinity at station NP1 (33.3), located in the center of the western subarctic gyre, was relatively higher than those at the other subarctic North Pacific stations (32.7–32.9). The water temperatures at stations NP1, NP3, and NP4 in the subarctic North Pacific rapidly decrease below the surface mixed layer and then gradually decreased below 100–200 m depth. Those at station NP2 in the subarctic North Pacific and at stations BS1–BS3 in the Bering Sea Basin stations were characterized by a warm surface layer from 0 to 30 m, a cold intermediate layer from 50 to 150–200 m, and a warm intermediate layer from 200 to 500–750 m (Figures 2a and 2c). The cold intermediate layer forms through two processes: the vertical mixing

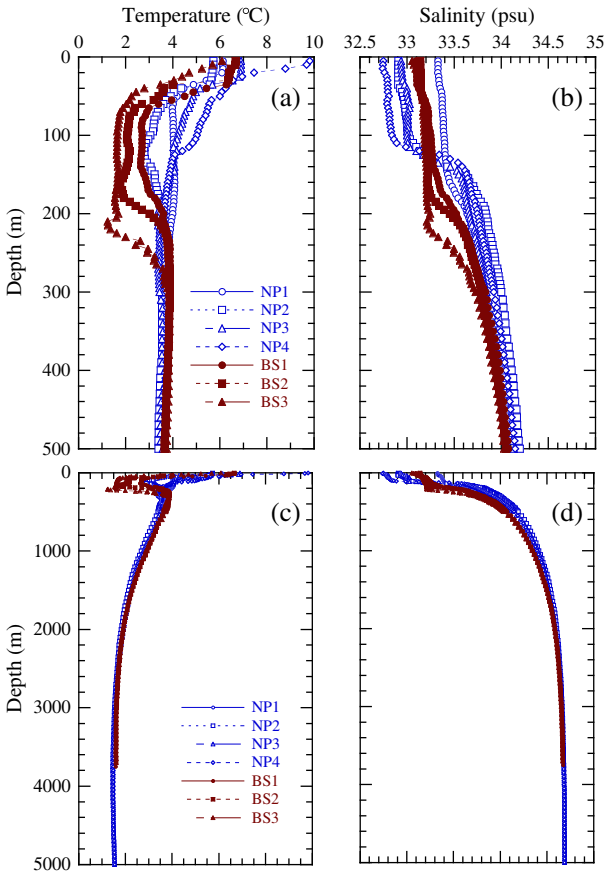

Figure 2. Vertical distributions of temperature (*T*) and salinity (*S*) in the surface water (a, b) and throughout the water column (c, d). Open blue symbols, stations NP1–NP4 along 47°N latitude in the subarctic North Pacific; solid red symbols, stations BS1–BS3 in the Bering Sea (Figure 1 and Table 1).

caused by the cooling of surface water in autumn and winter, and the warming of surface water in spring and summer. The lower temperature water, which is formed in the winter mixed layer, remains in the subsurface in the warming season [*Miura et al.*, 2002]. The temperature minimum layer is a characteristic feature of the North Pacific subarctic gyre and is particularly evident in the Bering Sea region [*Luchin et al.*, 1999; *Miura et al.*, 2002]. This layer overlies the strong halocline around 150–300 m depth in the Bering Sea (Figure 2b). Salinity at all stations in the subarctic North Pacific and the Bering Sea increased with depth (Figures 2b and 2d).

3.2. Iron and Other Biochemical Components in Surface Water of the Subarctic North Pacific and the Bering Sea

[11] In the surface mixed layer at all stations of the subarctic North Pacific (NP1–NP4) and stations BS1 and BS2 in the Bering Sea, macronutrient concentrations were high, within 14–18 μM for $NO_3 + NO_2$, 1.4–1.8 μM for PO_4, and 14–29 μM for $Si(OH)_4$ (Figure 3a–3c). However, the Si $(OH)_4$ concentration at station BS3 in the Bering Sea (1.4–2.0 μM) was one order of magnitude lower than those at other stations, whereas $NO_3 + NO_2$ and PO_4 concentrations were almost the same as those at other stations (Figure 3a–3c).

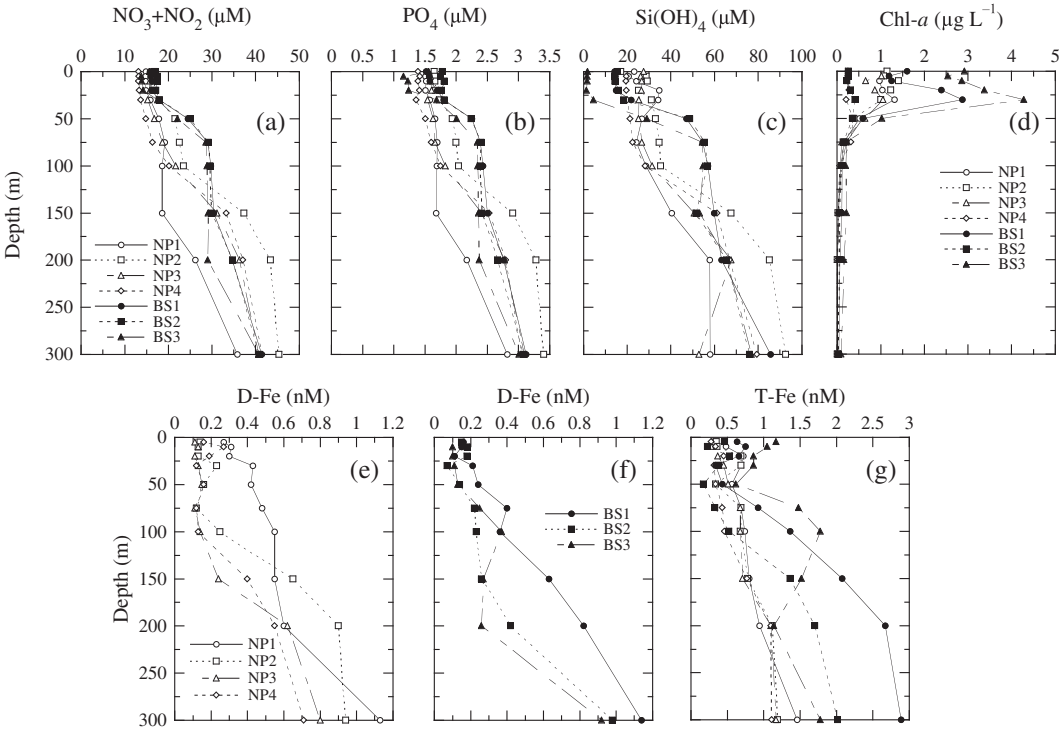

Figure 3. Vertical distributions of (a) $NO_3 + NO_2$, (b) PO_4, (c) $Si(OH)_4$, (d) Chl *a*, (e, f) D-Fe, and (g) T-Fe concentrations in the surface waters (≤300 m) of the subarctic North Pacific (open symbols, stations NP1–NP4 along 47°N latitude) and the Bering Sea (solid symbols, stations BS1–BS3).

In the surface mixed layer, Chl *a* concentrations were relatively high (2.9–4.3 μg L^{-1}) at stations BS1 and BS3 in the Bering Sea and relatively low (0.4–1.4 μg L^{-1}) at all stations of the subarctic North Pacific and at station BS2 in the Bering Sea (Figure 3d). Below the surface mixed layer, macronutrient concentrations in the subarctic North Pacific gradually increased with depth, whereas those in the Bering Sea rapidly increased with depth (Figure 3a–3c).

[12] Dissolved Fe concentrations in the surface mixed layer were relatively low, ranging from 0.1 to 0.3 nM at the subarctic North Pacific stations (Figure 3e) and from 0.1 to 0.2 nM at the Bering Sea stations (Figure 3f). The D-Fe concentrations in the surface mixed layer at stations NP2 and NP3 in the subarctic North Pacific (0.11–0.14 nM) and at stations BS1 and BS3 in the Bering Sea (0.10–0.16 nM) were lower than those at other stations. D-Fe in the surface water below the surface mixed layer tended to increase gradually with depth at all stations, except at station NP1, located in the center of the western subarctic gyre, where concentrations were consistently high throughout the surface water, ranging from 0.4 to 0.55 nM at 25–100 m (Figure 3e).

[13] Total Fe concentrations in the surface mixed layer were high, 0.3–0.7 nM, at the subarctic North Pacific stations and within a wide range of 0.2–1.2 nM at the Bering Sea stations (Figure 3g). The minimum values for T-Fe in the surface water were at 30–50 m depth at each Bering Sea station (0.4 nM at station BS1, 0.2 nM at BS2, and 0.7 nM at BS3, Figure 3g). The T-Fe below the surface mixed layer at the subarctic North Pacific stations increased gradually with depth to 1.1–1.5 nM at 300 m depth, whereas those at the Bering Sea stations tended to increase rapidly with depth to 1.8–2.8 nM at 300 m depth.

3.3. Iron and Other Chemical Components in the Deep Water of the Subarctic North Pacific and the Bering Sea

[14] At all stations in the subarctic North Pacific, the macronutrients except for $Si(OH)_4$, AOU, and humic F-intensity were generally low at the surface, high from 500 m to 1500 m, and decreased gradually in the deeper water below 1500 m (Figure 4). The vertical distributions and concentration of $NO_3 + NO_2$ in the deep waters of the Bering Sea were almost the same as those in the subarctic North Pacific (Figure 4a), whereas those of PO_4, $Si(OH)_4$, AOU, and humic F-intensity in the deeper water below 1500–2000 m in the Bering Sea were higher than those of the subarctic North Pacific (Figure 4b–4e). $Si(OH)_4$ concentrations in the Bering Sea increased with depth to a maximum value of approximately 210 μM at 3500 m depth and then decreased slightly to approximately 180 μM at 3700–3750 m near the bottom (Figure 4c). The humic F-intensity levels in the deeper water below 1000 m in the Bering Sea remained relatively constant, with high values of 0.20–0.21 RU (Figure 4e).

[15] At the western stations along 47°N latitude in the subarctic North Pacific (NP1 and NP2), D-Fe concentrations were generally high in intermediate water (1.3–1.6 nM at NP1 and 1.2–1.4 nM at NP2), and then decreased with depth to around 1.1 nM at NP1 and increased slightly with depth to around 1.4 nM at NP2 for deep water below 3500–4000 m (Figure 5a and 5b). However, D-Fe concentrations at the eastern stations (NP3 and NP4, Figure 5c and 5d) were lower in intermediate water (1.0–1.2 nM at NP3, 0.9–1.1 nM at NP4) and deep water below 4000 m (0.7–0.9 nM at NP3, 0.6–0.7 nM at NP4) than those at the western stations (NP1 and NP2). The D-Fe

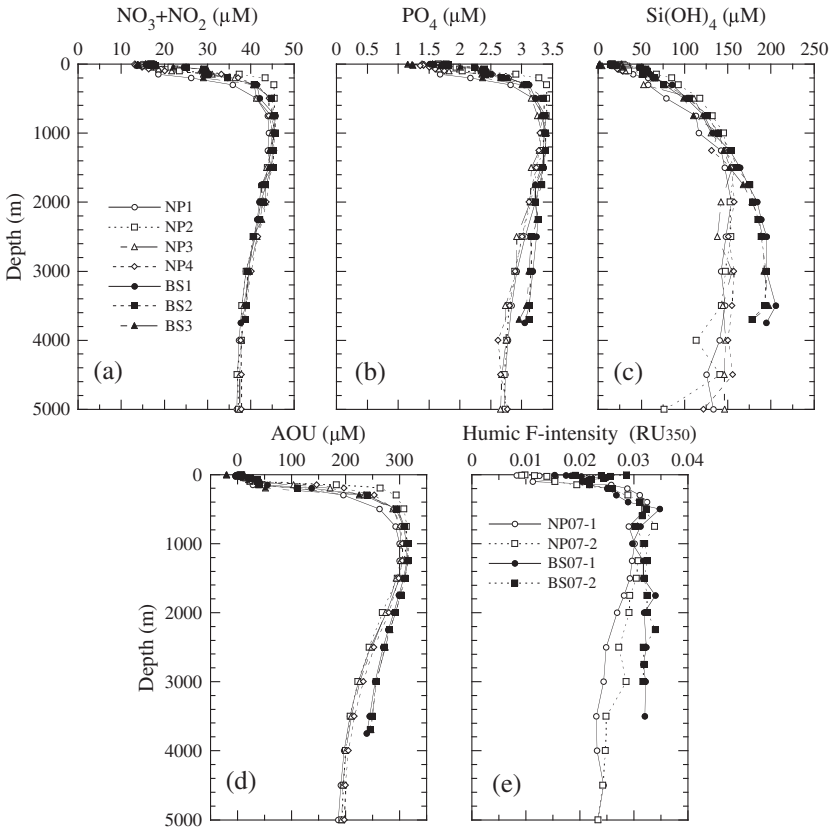

Figure 4. Vertical distributions of (a) $NO_3 + NO_2$, (b) PO_4, (c) $Si(OH)_4$, and (d) AOU throughout the water column of the subarctic North Pacific (open symbols, stations NP1–NP4 along 47°N latitude) and the Bering Sea (solid symbols, stations BS1–BS3). (e) Humic F-intensity (RU_{350}) throughout the water column of the subarctic North Pacific (open symbols, stations NP07-1 and NP07-2 in Figure 1 and Table 1) and the Bering Sea (solid symbols, stations BS07-1 and BS07-2 in Figure 1 and Table 1).

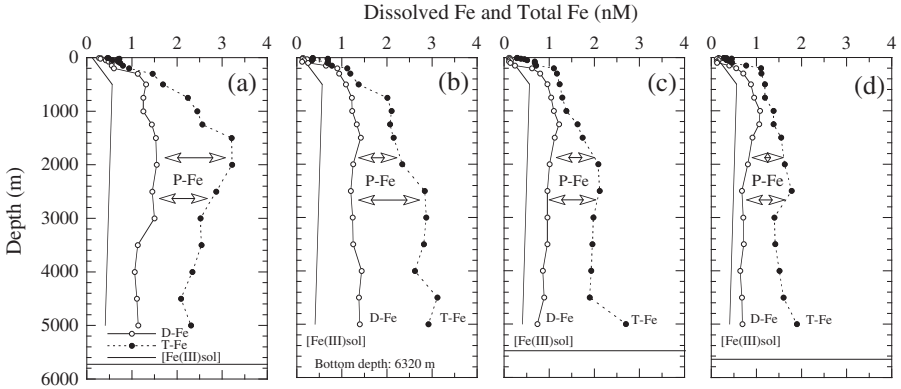

Figure 5. Vertical distribution of iron (open circles, D-Fe; solid circles, T-Fe; arrows, P-Fe [=T-Fe minus D-Fe]) throughout the water column at stations (a) NP1, (b) NP2, (c) NP3, and (d) NP4 along 47°N latitude in the subarctic North Pacific. Solid lines indicate the Fe(III) hydroxide solubility ([Fe(III)sol]) as estimated from the vertical distribution of humic F-intensity in the subarctic North Pacific (Figure 4e) and the linear equation for the relationship between [Fe(III)sol] and humic F-intensity in the central North Pacific Ocean ([Fe(III)sol][nM] = 18.833 × humic F-intensity [RU_{350}] − 0.045; $R = 0.78$, $n = 14$; *Kitayama et al.* [2009]).

maxima were 1.6 nM at 2000 m at NP1, 1.4 nM at 1500 m at NP2, 1.2 nM at 1250 m at NP3, and 1.1 nM at 1000 m at NP4. In terms of both depth and concentration, the D-Fe maxima decreased from west to east in the order NP1 > NP2 NP3 > NP4, indicating an eastward shoaling and decrease in the maximum D-Fe concentration.

[16] As with D-Fe, the vertical distribution of T-Fe at the western station (NP1) rapidly increased with depth in intermediate water and decreased slightly with depth in deep water (approximately 2–3 nM, Figure 5a). T-Fe in the intermediate and deep waters also followed an eastward decreasing trend (NP1 > NP2 > NP3 > NP4) from 3 to 2 nM (Figure 5).

[17] At all stations in the Bering Sea (BS1–BS3; Bowers and Aleutian Basins), D-Fe showed very similar depth profiles, with almost the same D-Fe concentration at each depth. The vertical profiles were characterized by a rapid increase with depth in mid-depth water (around 50–300 m) to approximately 1 nM at 300 m, a gradual increase with depth in intermediate water to a maximum of 1.6–1.7 nM at 1500–2250 m, and then a gradual decrease with depth in deep water to 1.3–1.4 nM at 3700 m (Figure 6). The deep water D-Fe maximum in the Bering Sea was deeper than in the subarctic North Pacific (Figures 5 and 6). Similarly, T-Fe concentrations tended to increase rapidly with depth in mid-depths to 2.5–3.2 nM at 500 m and then to gradually increase with depth in intermediate and deep waters to a maximum of approximately 3.5 nM at 3500 m at station BS1, at 2500 m at BS2, and at 1750–3000 m at BS3 (Figure 6). However, at all stations (BS1–BS3) T-Fe in bottom water below 3500 m tended to decrease with depth.

4. Discussion

4.1. Comparison between Iron and Other Biochemical Components in the Surface Water of the Subarctic North Pacific and the Bering Sea

[18] In the Bering Sea in summer reported nitrate and Chl *a* concentrations in the surface mixed layer (<20–30 m depth) are usually 10–25 μM and <1 μg L^{-1}, respectively [*Odate*, 1996; *Shiomoto et al*., 2002; *Takata et al*., 2005]. Previously *Takata et al*. [2005] observed low D-Fe and T-Fe concentrations (0.06–0.30 nM and 0.15–0.36 nM, respectively) and high nutrient concentrations (18–24 μM for $NO_3 + NO_2$, 1.4–1.9 μM for PO_4, and 23–43 μM for $Si(OH)_4$) at the depth of relatively low Chl *a* concentrations (0.6–1.0 μg L^{-1}) in the surface mixed layer (0–30 m depth) of the Bering Sea (53°29′N, 177°01′W, Figure 1) in the middle of July. Likewise *Aguilar-Islas et al*. [2007] pointed out high-nutrient, low-chlorophyll (HNLC) surface waters (15–20 μM for NO_3 and approximately 0.07 nM for D-Fe) in the oceanic region of the Bering Sea during summer, similar to other HNLC subarctic North Pacific regimes. In the present study, except for station BS3 we found relatively low D-Fe (0.1–0.3 nM for the subarctic North Pacific [Figure 3e] and 0.1–0.2 nM for the Bering Sea [Figure 3f]) and high nutrient concentrations (Figures 3a–3c), in the surface mixed layer (<20–40 m) of the subarctic North Pacific and the Bering Sea, probably resulting from effective biological uptake of atmospheric or laterally advected iron in the surface waters. However, we observed high Chl *a* concentrations (2–4.2 μg L^{-1}, Figure 3d) and relatively high T-Fe (0.7–1.2 nM, Figure 3g) in the surface mixed layer at stations BS1 and BS3 and remarkably low $Si(OH)_4$ concentrations (1.5–2 μM, Figure 3c) at station BS3 in late June and early July 2009. The high Chl *a* and high T-Fe concentrations in the surface mixed layer at stations BS1 and BS3 might be due to the unusually late spring phytoplankton bloom in 2009 or to a sporadic iron supply. The low Chl *a* and low T-Fe concentrations at station BS2, located in the centre of the basin gyre, could be due to a reduced iron supply from the shallower part of the basin.

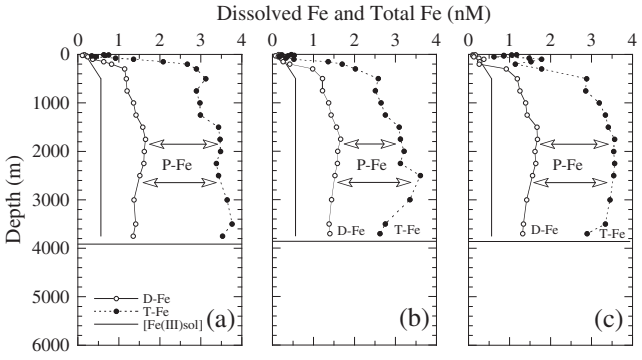

Figure 6. Vertical distribution of iron (open circles, D-Fe; solid circles, T-Fe; arrows, P-Fe [=T-Fe − D-Fe]) throughout the water column at stations (a) BS1, (b) BS2, and (c) BS3 in the Bering Sea. Solid lines indicate the Fe(III) hydroxide solubility ([Fe(III)sol]) as estimated from the vertical distribution of humic F-intensity in the Bering Sea (Figure 4e) and the linear equation for the relationship between [Fe(III) sol] and humic F-intensity in the central North Pacific Ocean ([Fe(III)sol][nM] = 18.833 × humic F-intensity [RU_{350}] 0.045; $R = 0.78$, $n = 14$; *Kitayama et al*. [2009]).

[19] At 50–150 m, below the surface mixed layer, the higher macronutrient concentrations in the Bering Sea compared to the subarctic North Pacific (Figure 3a–3c) are likely associated with the cold intermediate layer in the Bering Sea and probably result from the upward transport of nutrients during vertical mixing by cooling of the water in autumn and winter [*Miura et al*., 2002]. In surface waters below the surface mixed layer, D-Fe and T-Fe in the subarctic North Pacific and the Bering Sea increased rapidly with depth to relatively high and variable values (Figure 3e–3g). These rapid increases in D-Fe and T-Fe with depth and the iron concentrations measured in the present study are consistent with those from our previous studies in the western North Pacific (stations NP04-1, NP04-2, and NP04-3 at 41°N–47°N along 165°E longitude) and at a higher latitude in the central North Pacific (station NP04-4 at 50°N, 165°W; Figure 1) [*Takata et al*., 2006; *Kitayama et al*., 2009]. However, the iron concentrations in surface waters in the present study were higher than those at lower (29°N and 35°N, 165°W) and midlatitudes (NP04-5 and NP04-6 at 41°N–45°30′N along 165°W longitude; Figure 1) in the central North Pacific [*Takata et al*., 2006; *Kitayama et al*., 2009]. In particular, we observed relatively high T-Fe in the surface waters (including the surface mixed layer) at stations BS1 and BS3 and a subsurface T-Fe maximum value (1.8 nM) at 100 m at BS3 (Figures 3g and 6c). The relatively high and variable iron concentrations in the surface waters may be due to lateral transport of iron-rich water from the Alaskan Stream to higher latitudes of the central North Pacific (station NP04-4 at 50°N, 165°W; Figure 1; *Takata et al*. [2006]) and northward inflows of the Alaskan Stream through various passes to the ANSC [*Reed and Stabeno*, 1990] and from the continental shelf region in the eastern

Bering Sea to the BSC along the shelf slope [*Mizobata et al*., 2006; *Aguilar-Islas et al*., 2007; *Tanaka et al*., 2012].

[20] We calculated vertically integrated T-Fe and D-Fe inventories by interpolation between the data points from one depth to another in the upper 200 m (surface water) and upper 3500 m (throughout the water column) of the subarctic North Pacific (stations NP1–NP4) and the Bering Sea (stations BS1–BS3) (Figure 7). In the surface water, the T-Fe and D-Fe inventories at stations NP1–NP4 ranged from 114 to 143 μmol-Fe m^{-2} and from 43 to 97 μmol-Fe m^{-2}, respectively (Figure 7a). D-Fe inventories were approximately 50 ± 20% of the T-Fe. The T-Fe inventories along 47°N (stations NP1–NP4) in the present study were almost the same as those in the western North Pacific (stations NP04-1, NP04-2, and NP04-3) and the central high-latitude North Pacific (station NP04-4) regions in our previous studies [*Takata et al*., 2006; *Kitayama et al*., 2009] (Figure 1). However, they were 2–5 times those in the central low (29°N and 35°N, 165°W) and midlatitudes (stations NP04-5 and NP04-6 at 41°N–45°30′N along 165°W longitude) of the North Pacific in our previous studies [*Takata et al*., 2006; *Kitayama et al*., 2009]. In addition, the eastwardly decreasing trends in T-Fe and D-Fe inventories in the surface water along 47°N in the present study (Figure 7a) probably indicate a higher dust flux in the western region than the central region, although the effect of lateral transport of iron-rich water from the Alaskan Stream to the high-latitude North Pacific surface waters cannot be ignored.

[21] In the surface water of the Bering Sea (stations BS1–BS3), the T-Fe inventories are variable and ranged from 156 to 273 [228 ± 63 (±1SD)] μmol-Fe m^{-2}; D-Fe ranged from 45 to 87 [60 ± 23 (±1SD)] μmol-Fe m^{-2} (Figure 7a). The D-Fe inventories at stations BS1–BS3 were approximately 25 ± 7% of T-Fe and were very similar to those in the subarctic North Pacific (stations NP1–NP4), whereas the T-Fe inventories at BS1 and BS3 were approximately double those at BS2 and in the subarctic North Pacific. The high T-Fe inventories at stations BS1 and BS3 are probably due to the lateral transport of iron-rich water from the ANSC and BSC, respectively, rather than aeolian iron input. In a previous study [*Fujita et al*., 2010], we observed notably higher T-Fe inventories in the surface water of the semienclosed Japan Sea at locations close to the western Japanese coast than in the central Japan Sea, resulting from the subsurface supply of iron remobilized or resuspended from continental shelf sediments [*Johnson et al*., 1999; *Elrod et al*., 2004; *Lam and Bishop*, 2008].

[22] Because iron is preferentially scavenged from the water column during the mineralization cycle, upwelled oceanic water is relatively deficient in iron compared to nitrogen species. Upwelling and vertical mixing will bring water with high N:D-Fe ratio (>30,000:1) to the surface [*Brown et al*., 2005]. Therefore, surface waters require additional iron input to reestablish the biologically required N/D-Fe balance. We calculated the C:Fe ratios in phytoplankton ($2.4–2.9 \times 10^5$:1 for NP1–NP4 and 2.1×10^5:1 for all BS stations) from the slopes of each linear relationship between AOU and D-Fe, due to iron release through the oxidative decomposition of sinking biogenic organic matter in deep water, in the upper 1000 m of the subarctic North Pacific and Bering Sea (Figure 8) and the Redfield ratio ($C/N/P/O_2 = 106:16:1:138$, *Redfield et al*. [1963]). Therefore, we used 30,000–45,000:1 as a maximum stoichiometric N/D-Fe mole ratio that allows the complete consumption of N; this ratio was calculated by assuming a limiting C/Fe ratio in phytoplankton of $2–3 \times 10^5$:1 [this study; *Takeda*, 2011] and a C/N ratio of 6.7:1. In the present study, we found N/D-Fe ratio >40,000:1 in the upper 50 m of surface waters in the subarctic North Pacific and Bering Sea (40,000–55,000:1 at NP1, 50,000–150,000:1 at NP2–NP4, and 85,000–250,000:1 at BS1–BS3) (Figures 3a, 3e, and 3f, and 8), implying that the surface waters are iron-limited

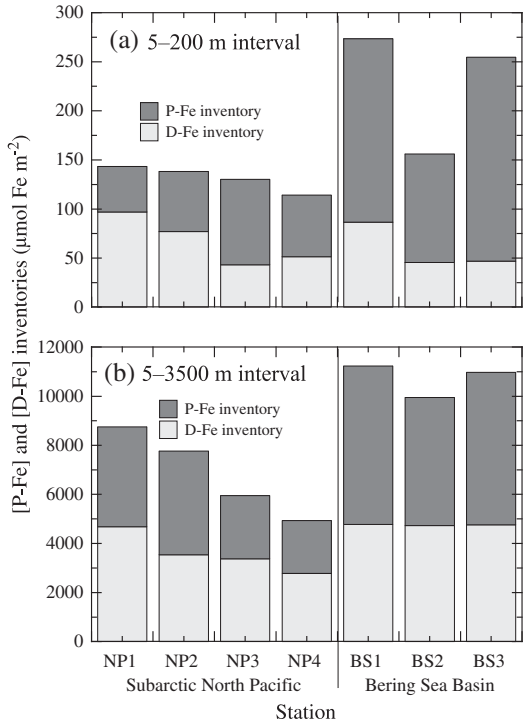

Figure 7. Vertically integrated P-Fe and D-Fe (T-Fe = P-Fe + D-Fe) inventories in the (a) upper 200 m and (b) upper 3500 m of the subarctic North Pacific (stations NP1–NP4) and the Bering Sea (stations BS1–BS3).

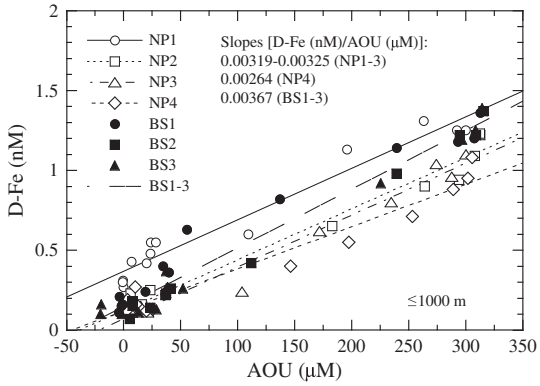

Figure 8. D-Fe concentration versus AOU in the upper 1000 m of the subarctic North Pacific (open symbols, stations NP1–NP4) and the Bering Sea (solid symbols, stations BS1–BS3).

in the presence of sufficient nitrate. The absence of atmospheric and fluvial iron inputs tends to increase the N/D-Fe ratio in surface waters. However, atmospheric and fluvial input of D-Fe are reportedly less important than vertical mixing in maintaining high N/D-Fe ratios in the HNLC surface waters of the western North Pacific subarctic gyre [*Brown et al*., 2005; *Measures et al*., 2005]. Iron input into the surface waters of the Bering Sea is therefore insufficient to allow the consumption of the entire nitrate + nitrite pool, although we measured relatively higher surface Chl *a* and T-Fe at stations BS1 and BS2 (Figure 3).

[23] In mid-depth waters (200–500 m) in the study area, the similarities between vertical profiles of nutrient concentrations, AOU, humic F-intensity, D-Fe, and T-Fe (Figures 3–6) suggest that they are controlled by similar biogeochemical and physical processes. The increases in D-Fe and T-Fe with depth are strongly related to the remineralization of sinking particulate organic matter, as is AOU, humic-type FDOM, and the regeneration of nutrients. In our previous studies [*Takata et al*., 2006; *Kitayama et al*., 2009], we reported that the northwardly increasing trends in D-Fe, T-Fe, and nutrient concentrations in mid-depth waters of the western and central North Pacific are due to the effect of northward upwelling and the higher biological productivity and degradation of particulate organic matter at higher latitude. In addition, the more rapid increases in D-Fe and T-Fe with depth and their higher concentrations in mid-depth waters of the Bering Sea than in the subarctic North Pacific (Figures 5 and 6) probably result from higher biological productivity in the Bering Sea region. Long-term observations from time series sediment traps in the Aleutian Basin of the Bering Sea (53°30′N, 177°W; Figure 1) and the central subarctic North Pacific (49°N, 174°W) have shown that total mass fluxes consist primarily of biogenic phases, and diatom fluxes in the Bering Sea were approximately double those in the subarctic North Pacific because of the higher biological productivity in the Bering Sea [*Takahashi et al*., 2000, 2002].

4.2. Iron and Other Chemical Components in the Deep Water of the Subarctic North Pacific Ocean

[24] Concentrations of $NO_3 + NO_2$, PO_4, $Si(OH)_4$, humic F-intensity and AOU, and their vertical distributions in deep waters were invariant in the subarctic North Pacific (Figure 4). However, the vertically integrated inventories of D-Fe and T-Fe in the upper 3500 m of the subarctic North Pacific (stations NP1–NP4 along 47°N) ranged from 2800 to 4700 μmol-Fe m^{-2} and from 4900 to 8700 μmol-Fe m^{-2}, respectively (Figure 7b). We calculated labile particulate Fe (P-Fe, >0.22 μm fraction) as T-Fe minus D-Fe, and inventories at stations NP1–NP4 ranged from 2100 to 4000 μmol-Fe m^{-2} in the upper 3500 m (Figure 7b). D-Fe inventories were approximately 50 ± 5% of T-Fe. These D-Fe, T-Fe, and P-Fe inventories all appeared to follow the trend of eastward decrease. The D-Fe, T-Fe, and P-Fe concentrations in intermediate and deep waters also showed eastwardly decreasing trends (NP1 > NP2 > NP3 > NP4, Figures 5 and 9a–9c). In addition, we observed an eastwardly shallower D-Fe maximum and deeper T-Fe maximum in

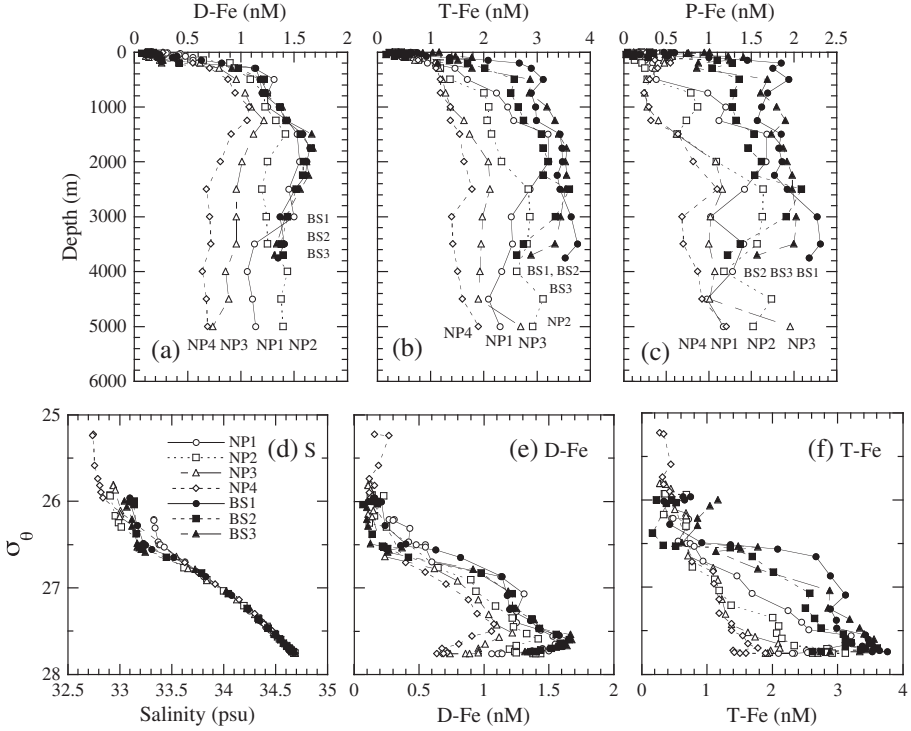

Figure 9. Comparison between the vertical distributions of (a) D-Fe, (b) T-Fe, and (c) P-Fe in the subarctic North Pacific (open symbols, stations NP1–NP4) and the Bering Sea (solid symbols, stations BS1–BS3). (d–f) concentrations of $NO_3 + NO_2$ (d), D-Fe (e), and T-Fe (f) versus potential density (σ_θ) in the subarctic North Pacific (open symbols, stations NP1–NP4) and the Bering Sea (solid symbols, stations BS1–BS3).

intermediate and deep waters except for bottom water (Figures 5, 9a and 9b).

[25] In this study, profiles of $NO_3 + NO_2$, D-Fe, and T-Fe versus potential density (σ_θ) in the subarctic North Pacific commonly showed strong gradients in the σ_θ range of 26.5–27.3 (Figure 9d–9f). The $NO_3 + NO_2$ concentrations had almost the same maxima within a narrow σ_θ range of 27.3–27.5 (Figure 9d). However, the D-Fe and T-Fe maxima appeared at higher σ_θ (27.4–27.7) and were somewhat scattered with an eastward decrease (Figure 9e and 9f). In deep waters of the subarctic North Pacific, there are large differences between stations (NP1–NP4 along 47°N) in D-Fe and T-Fe, but nutrient concentrations and AOU varied little (Figures 4, 5 and 9). This suggests that iron concentrations respond on a shorter time scale than nutrients or AOU. The nutrient and iron depth profiles appeared more decoupled in the deeper waters, suggesting iron removal by particle scavenging.

[26] Previous studies also observed high concentrations of D-Fe, T-Fe, and P-Fe in intermediate and deep waters of the western North Pacific (for example, at stations NP04-1, NP04-2, and NP04-3 at 41°N–47°N along 165°E; Figure 1) and at high latitude in the central North Pacific (station NP04-4 at 50°N, 165°E; Figure 1) [*Nakabayashi et al*., 2001; *Nishioka et al*., 2003, 2007; *Takata et al*., 2005, 2006; *Kitayama et al*., 2009]. However, iron concentrations much lower than those in the western North Pacific were observed in the central North Pacific at low latitudes (29°N and 35°N along 165°W, and 28°N, 155°W; *Bruland et al*. [1994]; *Kitayama et al*. [2009]) and midlatitudes (stations NP04-5 and NP04-6 at 41°N–45°30′N along 165°W [Figure 1]; *Takata et al*. [2006]; *Kitayama et al*. [2009]) and in the Gulf of Alaska (50°N, 145°W; *Martin et al*. [1989]; *Johnson et al*. [1997a]; *Nishioka et al*. [2001, 2003]). The higher iron concentrations in the western than the central and eastern North Pacific reflect the regional patterns of eolian source, physical transport, and the water column processes involved in the cycling of iron, such as biological uptake, remineralization of biogenic matter, scavenging onto particles, and Fe(III) hydroxide solubility, which is controlled by iron complexation with natural organic ligands [*Rue and Bruland*, 1995; *Kuma et al*., 1996, 2003; *Croot and Johansson*, 2000; *Tani et al*., 2003; *Kitayama et al*., 2009; *Boyd and Ellwood*, 2010; *Gledhill and Buck*, 2012]. Therefore, the characteristic trend of eastwardly decreasing iron inventory in the water column (Figure 7b) and iron concentrations with eastwardly shallower D-Fe maxima and deeper T-Fe maxima (Figures 5 and 9) probably results from the higher input of dissolved Fe in the western region because of higher atmospheric or lateral iron inputs. The eastward decrease in D-Fe, T-Fe, and P-Fe in the deep water of the subarctic North Pacific may be due to the removal of colloidal Fe (including in D-Fe, i.e., the <0.22 μm fraction) as well as particulate Fe (>0.22 μm fraction) by particle scavenging during the eastward transport of deep water [*Bergquist et al*., 2007; *Kitayama et al*., 2009]. However, the time scales of the water mass flow and scavenging of the colloidal Fe fraction are still unknown.

[27] In near-bottom waters at stations NP1, NP3, and NP 4, the trend of increasing T-Fe with depth (Figures 5a, 5c and 5d) is probably due to the resuspension of sediments from the seafloor. Previous studies observed this increasing trend over a wide area of the North Pacific [*Ezoe et al*., 2004; *Takata et al*., 2005; *Kitayama et al*., 2009], although D-Fe in deep and bottom waters gradually decreased with depth and followed the trend of eastward decrease.

4.3. Chemical Components in the Deep Water of the Bering Sea

[28] There were no differences in the vertical distributions or levels of $NO_3 + NO_2$, PO_4, $Si(OH)_4$, AOU, and humic F-intensity in the intermediate and deep waters of the Bering Sea (Figure 4). However, concentrations of PO_4 and $Si(OH)_4$, AOU, and humic F-intensity in waters deeper than 1500–2000 m in the Bering Sea were clearly higher than those in the subarctic North Pacific (Figures 4b–4e), although there was no difference in the $NO_3 + NO_2$ concentrations between the subarctic North Pacific and the Bering Sea in the deep waters below 1500–2000 m depth (Figure 4a). Similarly, profiles of PO_4, $Si(OH)_4$, AOU, and humic F-intensity against σ_θ also showed that at $\sigma_\theta \geq 27.5$ (below 1500 m depth), levels in the Bering Sea were clearly higher than those in the subarctic North Pacific (data not shown), whereas $NO_3 + NO_2$ concentrations were almost the same (Figure 9d). The differences between PO_4, $Si(OH)_4$, AOU, and humic F-intensity in waters deeper than 1500–2000 m in the subarctic North Pacific and the Bering Sea increase with depth up to 3500 m, near bottom. These differences in deep water are due to the high biological productivity and high nutrient regeneration rates in the Bering Sea [*Saino et al*., 1979; *Tsunogai et al*., 1979]. Humic-type FDOM is produced in the water column by the oxidation and remineralization of settling organic particles and is destroyed by photochemical degradation in the surface waters [*Hayase et al*., 1988; *Chen and Bada*, 1992]. In deep water below 500 m, the slopes of the relationships between $NO_3 + NO_2$ concentration and AOU and between $NO_3 + NO_2$ and PO_4 concentrations (i.e., the $[NO_3 + NO_2]/[PO_4]$ ratio) in the Bering Sea are notably steeper than those in the subarctic North Pacific (Figures 10a and 10b). However, there is no clear difference in the two oceanic regions between the slopes of the relationship between PO_4 concentrations and AOU in deep waters (Figure 10c).

[29] Although there have been a number of studies of sedimentary denitrification on the Bering Sea shelf [e.g., *Hirota et al*., 2009; *Mordy et al*., 2010; *Granger et al*., 2011], a few studies have confirmed an apparent nitrate deficiency in the deep Bering Sea based on normalization to phosphate [*Broecker and Peng*, 1982; *Lehmann et al*., 2005; *Granger et al*., 2011], similar to our observations. Benthic denitrification has been suggested as the dominant cause for this nitrate deficiency [*Tsunogai et al*., 1979; *Broecker and Peng*, 1982]. Although we did not measure ammonium in the present study, *Lehmann et al*. [2005] reported that ammonium in the deep Bering Sea was always close to detection limits as measured onboard with a phenol-hypochlorite protocol. In the present study, we found $[NO_3 + NO_2]/[PO_4]$ ratios that were clearly different between the subarctic North Pacific and Bering Sea in waters deeper than 1500 m, but without a clear difference at 500–1500 m (Figure 10b), suggesting substantial denitrification in deep waters. Additionally, we used the tracer N*, which is defined as $([NO_3^-] + [NO_2^-] - 16[PO_4^{3-}] + 2.9) \times 0.87$ in this study, to detect deviations in the ratio of $[NO_3 + NO_2]$ to $[PO_4]$, from

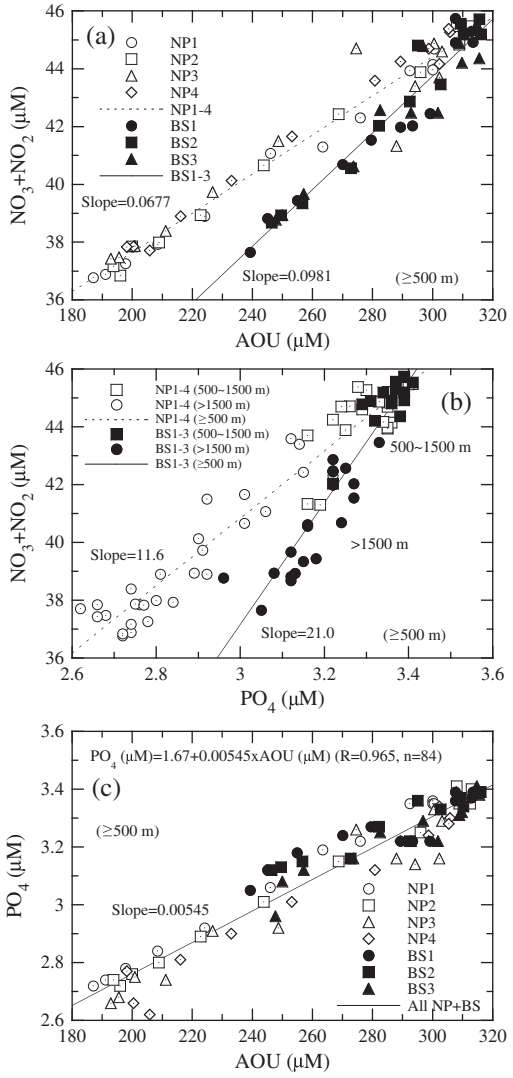

Figure 10. (a) $NO_3 + NO_2$ concentration versus AOU, (b) $NO_3 + NO_2$ concentration versus PO_4 concentration, and (c) PO_4 concentration versus AOU in deep water (≥500 m) in the subarctic North Pacific (open symbols, stations NP1–NP4) and the Bering Sea (solid symbols, stations BS1–BS3).

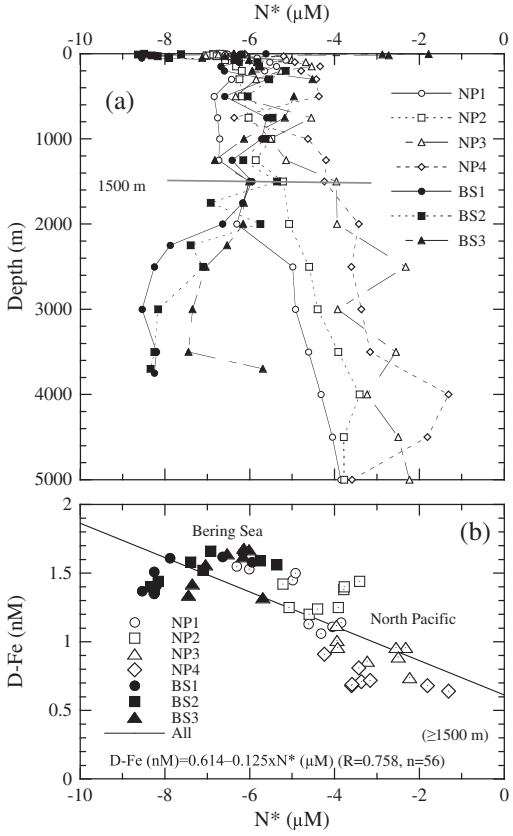

Figure 11. (a) Vertical distribution of N* throughout the water column and (b) D-Fe concentration versus N* in deep water (≥1500 m) of the subarctic North Pacific (open symbols, stations NP1–NP4) and the Bering Sea (solid symbols, stations BS1–BS3).

those expected from the internal N cycle, given Redfield stoichiometry [*Gruber and Samiento*, 1997; *Yoshikawa et al*., 2006]. Generally, negative N* in the ocean interior indicates a net loss of nitrate, most likely due to denitrification. Consistent with earlier work [*Lehmann et al*., 2005; *Granger et al*., 2011], a very low N* (−6 to −9 μM in this study) was observed in the deeper waters below 1500 m in the Bering Sea Basin, while the low N* was not observed in the deep subarctic North Pacific (Figure 11a). *Lehmann et al*. [2005] have reported that the elevated average sediment denitrification rate of the deep Bering Sea is driven by organic matter supply to the base of the continental slope, owing to a combination of high primary productivity in the surface waters along the shelf break and efficient downslope sediment focusing along the steep continental slopes that characterize the Bering Sea.

4.4. Iron in the Deep Water of the Bering Sea

[30] At the stations BS1–BS3 in the Bering Sea, D-Fe, T-Fe, and P-Fe in deep water showed very similar patterns with depth, especially in the consistently high D-Fe concentrations at each depth. The D-Fe distribution was characterized by a rapid increase with depth in mid-depths, a gradual increase with depth in intermediate water up to the maximum of 1.6–1.7 nM at 1500–2250 m, and then a gradual decrease with depth in deep water to 1.3–1.4 nM at 3700 m (Figure 6). The vertically integrated T-Fe and D-Fe inventories over the upper 3500 m were nearly the same at the three Bering Sea stations, ranging from 10,000 to 11,200 [$10{,}720 \pm 680$ (±1SD)] μmol-Fe m^{-2} and from 4700 to 4800 [4760 ± 30 (±1SD)] μmol-Fe m^{-2} (Figure 7b). D-Fe inventories were approximately 45% ± 2% of T-Fe. T-Fe and P-Fe inventories in the Bering Sea were 1.5–2 times those in the subarctic North Pacific. In addition, profiles of D-Fe and T-Fe versus σ_θ in the Bering Sea (Figures 9e and 9f) show strong gradients in the σ_θ range from 26.5 to 27.6 and maxima at nearly the same σ_θ of 27.6–27.7.

[31] The iron concentrations and distributions with depth observed in the present study are similar to those found in the southeastern Aleutian Basin (station BS07-1 at 53°30′N, 177°W; Figure 1) in our previous study [*Takata et al*., 2005], but are generally higher than those in the

subarctic North Pacific (station NP1–NP4, Figures 9a and 9b) and those previously measured in the western North Pacific [*Takata et al*., 2006; *Kitayama et al*., 2009]. The characteristic depth regime (higher iron concentrations and deeper D-Fe maximum at 1500–2250 m) and higher iron inventory in the water column of the Bering Sea as compared with the North Pacific (Figures 5, 6, and 7b) are probably due to the higher biological productivity in surface water and the higher and deeper recycled D-Fe from the decomposition of sinking particulate organic matter in deep water. The high biological productivity in surface water of the Bering Sea can be attributed to iron input from the surrounding shelves and the passes in the Aleutian Island arc.

[32] The differences between D-Fe and T-Fe as well as PO_4, $Si(OH)_4$, AOU, and humic F-intensity in the subarctic North Pacific and the Bering Sea deep waters (Figures 4–6, and 9) are probably due to the semiclosed nature of the Bering Sea, which severely restricts waters exchange with the neighboring Pacific Ocean. Most of the transport into the Bering Sea occurs through Near Strait with a sill depth of approximately 2000 m, and the Bering Sea inflow is balanced by outflow through the Kamchatka Strait with a sill depth of approximately 4000 m; the majority of the outflow from the Bering Sea to the subarctic North Pacific occurs through the Kamchatka Strait. In addition, the Kamchatka Strait is the only conduit into the Bering Sea that is deep enough (>2000 m) to permit inflow of Deep Pacific Water [*Reed et al*., 1993; *Stabeno et al*., 1999]. Deep water exchange with the adjacent subarctic North Pacific probably occurs at a low rate, resulting in hydraulic residence times of approximately 300–400 years for the deep Bering Sea [*Tsunogai et al*., 1979; *Coachman et al*., 1999]. It is likely that the rate of Bering Sea deep water exchange (below around 1500–2000 m) is substantially lower than that for the water above, although few data are available on deep circulation in the Bering Sea. Therefore, the observations that the depth regime of D-Fe is almost the same throughout Bering Sea deep waters and that the Bering Sea has higher and deeper inputs of D-Fe (maximum values of 1.6–1.7 nM at 1500–2250 m depth) as well as PO_4 and humic F-intensity than the subarctic North Pacific deep waters can probably be explained by a longer accumulation time for decomposition or transformation products by high-productivity surface waters and inordinately slow replacement of deep basin waters. In addition, we found a relatively significant relationship between D-Fe and N* in deep waters below 1500 m in the Bering Sea Basin and the subarctic North Pacific (Figure 11b), resulting in the increase in D-Fe with decreasing N* (Figure 11b). It may be suggested that the excess D-Fe in the Bering Sea deep waters is supplied from the organic-rich downslope sediment focusing along the steep continental slopes that characterize the Bering Sea [*Lehmann et al*., 2005].

[33] In Bering Sea bottom water from 3500 to 3700 m, we observed rapid decreases with depth in T-Fe and P-Fe as well as $Si(OH)_4$ concentrations (Figures 4, 6c, 6, and 9), probably resulting from bottom water renewal. A previous study in the Bering Sea suggested that rapidly decreasing $Si(OH)_4$ and increasing oxygen with depth in bottom water indicated that bottom water was more recently exposed to the ocean surface than the water above [*Coachman et al*., 1999]. The source for Bering Sea bottom water below about 3500 m is North Pacific water from depths around 3500–4000 m, which enters through the sill-less Kamchatka Strait and flows sequentially through the Kamchatka Basin into the Bowers and Aleutian Basins. The bottom water renewal slowly displaces upward the deep water layers; the water is ultimately removed from the Bering Sea by circulation as depths <2000 m [*Coachman et al*., 1999].

4.5. Relationship between Iron and Humic-type FDOM in the Deep Water of the Subarctic North Pacific and the Bering Sea

[34] Several types of Fe organic complexes in seawater ranged from high affinity siderophores present at low concentrations [e.g., *Gledhill et al*., 2004; *Mawji et al*., 2011; *Velasquez et al*., 2011] to weaker but more abundant less well-defined organic compounds such as humic substances (HS) and exopolysaccharides (EPS) with complex molecules [e.g., *Kitayama et al*., 2009; *Laglera and van den Berg*, 2009; *Hassler et al*., 2011a, 2011b; *Croot and Heller*, 2012; *Gledhill and Buck*, 2012]. The HS fraction is quite refractory and persists into the deep ocean, while EPS is likely to be produced in surface waters as it is associated with phytoplankton productivity. However, it is still poorly characterized for the association between Fe, HS and EPS, and the contribution of HS and EPS to the ambient ligand pool in the open ocean [*Gledhill and Buck*, 2012].

[35] In our previous studies [*Tani et al*., 2003; *Takata et al*., 2004, 2005; *Kitayama et al*., 2009; *Yamashita et al*., 2010], we observed a strong linear correlation between D-Fe (<0.22 μm fraction) and humic F-intensity in the central deep North Pacific Ocean, and relatively similar linear relationships between Fe(III) hydroxide solubility ([Fe(III)sol], <0.025 μm fraction) and humic F-intensity in the deep water column of the marginal seas and oceanic regions of the North Pacific. Humic-type FDOM has been suggested as controlling [Fe(III)sol] by functioning as natural organic ligands that form complexes with Fe(III) and therefore may be responsible for D-Fe in the deep water column [*Tani et al*., 2003; *Kitayama et al*., 2009; *Yamashita et al*., 2010]. However, relatively high [Fe(III)sol] has been often observed in the euphotic zone [e.g., *Kuma et al*., 1998; *Nakabayashi et al*., 2002; *Tani et al*., 2003; *Takata et al*., 2004; *Kitayama et al*., 2009; *Schlosser et al*., 2012], where the humic fluorescence signal is attenuated in the surface waters due to photobleaching [e.g., *Hayase et al*., 1988; *Chen and Bada*, 1993; *Murphy, et al*., 2008]. Therefore, the high [Fe(III)sol] in oceanic surface waters is probably controlled by the presence of strong Fe-binding organic ligands, such as siderophores [*Kuma et al*., 1996; *Tani et al*., 2003; *Kitayama et al*., 2009, *Schlosser and Croot*, 2009; *Heller et al*., 2012]. In the present study, the humic F-intensity values in the surface waters of the Bering Sea (station BS07-1, which is far from the eastern Bering shelf region) and the northern North Pacific (stations NP07-1 and NP07-2) ranged from 0.008 to 0.020 RU_{350} (Figure 4e), very similar to those of the Pacific and Atlantic surface waters (0.005 to 0.020 RU_{350}, *Murphy et al*. [2008] and *Heller et al*. [2012]). However, the humic F-intensity values in deep water of the Bering Sea (0.030–0.035 RU_{350}) were higher than those of the subarctic North Pacific (0.023–0.032 RU_{350}) (Figure 4e).

[36] By using a linear equation for the relatively linear relationship between [Fe(III)sol] and humic F-intensity in the central deep North Pacific Ocean ([Fe(III)sol][nM] =

$18.833 \times$ humic F-intensity $[RU_{350}] - 0.045$; $R = 0.78$, $n = 14$; *Kitayama et al*. [2009]) and the vertical distributions of humic F-intensity in the subarctic North Pacific (stations NP07-1 and NP07-2) and the Bering Sea (stations BS07-1 and BS07-2) (Figure 4e), we estimated [Fe(III)sol] profiles for the water column of both regions (solid lines in Figures 5 and 6), although more information in other basins needs to be provided supporting the wider application of this relationship between [Fe(III)sol] and humic F-intensity. We used these estimates to decide whether the D-Fe in deep water of the subarctic North Pacific and the Bering Sea found in the present study can be attributed to a solubility near-equilibrium between soluble Fe and Fe(III) hydroxide in seawater. The D-Fe values (0.7–1.5 nM, <0.22 μm fraction) in deep waters of the subarctic North Pacific were higher than the [Fe(III)sol] value (0.41–0.57 nM, <0.025 μm fraction), but trended eastwardly toward the [Fe(III)sol] line (Figure 5). However, the D-Fe values in the Bering Sea deep waters (1.3–1.7 nM) were notably much higher than the [Fe(III)sol] value (0.54–0.57 nM, Figure 6). Higher D-Fe than [Fe(III)sol] in the deep water of the Bering Sea would be regulated by the balance between the supply of dissolved Fe from remineralization of biogenic particles and Fe removal from scavenging in the ocean interior [*Kuma et al*., 2003; *Kitayama et al*., 2009]. Excess D-Fe relative to [Fe(III)sol] is probably due to the supply rate of dissolved Fe exceeding the removal rate and to the presence of Fe in colloidal form in the dissolved Fe fraction (<0.22 μm size) [e.g., *Nishioka et al*., 2001, 2003, 2005; *Cullen et al*., 2006; *Bergquist et al*., 2007; *Boye et al*., 2010]. The colloidal Fe is a significant portion of the dissolved organic Fe pool in the oceanic deep waters. It has been reported that vertical variations in dissolved Fe (<0.4 μm size) in the deep subtropical and tropical Atlantic Ocean are dominated by changing colloidal Fe (0.02–0.4 μm size) and little variability in soluble Fe (<0.02 μm size) [*Bergquist et al*., 2007]. The high dissolved Fe and colloidal Fe in deep oceanic waters is likely due to high iron input and remineralization of Fe-replete sinking organic matter under high productivity regions.

[37] The surface circulation in the Bering Sea Basin is a cyclonic gyre that includes the southward flowing Kamchatka Current (Figure 1), which flows southward along the Kuril Islands and contributes to the Oyashio. The flow in the upper 1500 m is dominated by the southward flowing Kamchatka Current on the western side of the Kamchatka Strait, which is the location of the majority of Bering Sea outflow [*Stabeno and Reed*, 1994]. Furthermore, high concentrations of $Si(OH)_4$ between 2000 m and 3000 m depths on the western side of the Kamchatka Strait suggest a southward flow of deep Bering Sea water beneath the Kamchatka Current [*Reed et al*., 1993]. Therefore, the distributions of iron and nutrients in the water column of the subarctic northwestern North Pacific, and particularly in the Oyashio region, are probably reflected by their high concentrations in the Bering Sea Basin.

[38] **Acknowledgments.** We thank K. Toya, Y. W. Watanabe, J. Nishioka, and K. Ono for their technical support and the captain and crew of the (T/V) *Oshoro-Maru* of Hokkaido University for their help in sampling. This work was supported by a Grant for Scientific Research (18201001) from the Ministry of Education, Culture, Sports, Science and Technology of Japan.

References

Aguilar-Islas, A. M., M. P. Hurst, K. N. Buck, B. Sohst, G. J. Smith, M. C. Lohan, and K. W. Bruland (2007), Micro- and macronutrients in the southeastern Bering Sea: Insight into iron-replete and iron depleted regimes, *Pro. Oceanogr.*, *73*, 99–126.

Bergquist, B. A., J. Wu, and E. A. Boyle (2007), Variability in oceanic dissolved iron is dominated by the colloidal fraction, *Geochim. Cosmochim. Acta*, *71*, 2960–2974, doi: 10.1016/j.gca.2007.03.013.

Boyd, P. W., and M. J. Ellwood (2010), The biogeochemical cycle of iron in the ocean. *Nat. Geosci.*, *3*, 675–682.

Boye, M., J. Nishioka, P. L. Croo, P. Lann, K. R. Timmermans, V. H. Strass, S. Takeda, H. J. W. de Baar (2010), Significant portion of dissolved organic Fe complexes in fact is Fe colloids. *Mar. Chem.*, *122*, 20–27.

Broecker, W. S., and T.-H. Peng (1982), Tracers in the Sea, Lamont-Doherty Geol. Obs., Palisades, New York.

Brown, M. T., W. N. Landing, and C. I. Measures (2005), Dissolved and particulate Fe in the western and central North Pacific: Results from the 2002 IOC cruise, *Geochem. Geophys. Geosyst.*, *6*, Q10001, doi: 10.1029/2004GC000893.

Bruland, K. W., and E. L. Rue (2001), Analytical methods for the determination of concentrations and speciation of iron, in The Biogeochemistry of Iron in Seawater, edited by D. R. Turner and K. A. Hunter, pp. 255–289, John Wiley, New York.

Bruland, K. W., K. J. Orians, and J. P. Cowen (1994), Reactive trace metals in the stratified central North Pacific, *Geochim. Cosmochim. Acta*, *58*, 3171–3182, doi: 10.1016/0016–7037(94)90044-2.

Chen, R. F., and J. L. Bada (1992), The fluorescence of dissolved organic matter in seawater, *Mar. Chem.*, *37*, 191–221.

Coachman, L. K., T. E. Whiteledge, and J. J. Goering (1999), Silica in Bering Sea deep and bottom water, in Dynamics of the Bering Sea, edited by T. R. Loughlin and K. Ohtani, pp. 285–309, University of Alaska Sea Grant, Fairbanks, Alaska.

Croot, P. L., and M. Johansson (2000), Determination of iron speciation by cathodic stripping voltammetry in seawater using the competing ligand 2-(2-thiazolylazo)-p-cresol (TAC), *Electroanalysis 12*, 565–576.

Croot, P. L., and M. I. Heller (2012), The important of kinetics and redox in the biogeochemical cycling of iron in the surface ocean, *Front. Microbiol.*, *3*, doi: 10.3389/fmicb.2012.00219.

Cullen, J. T., B. A. Bergquist, and J. W. Moffett (2006), Thermodynamic characterization of the partitioning of iron between soluble and colloidal species in the Atlantic Ocean. *Mar. Chem.*, *98*, 295–303.

Elrod, V. A., W. M. Berelson, K. H. Coale, and K. S. Johnson (2004), The flux of iron from continental shelf sediments: A missing source for global budgets, *Geophys. Res. Lett.*, *31*, L12307, doi: 10.1029/2004GL020216.

Ezoe, M., T. Ishita, M. Kinugasa, X. Lai, K. Norisuye, and Y. Sohrin (2004), Distributions of dissolved and acid-dissolvable bioactive trace metals in the North Pacific Ocean, *Geochem. J.*, *38*, 535–550.

Fujishima, Y., K. Ueda, M. Marumo, E. Nakayama, C. Tokutome, H. Hasegawa, M. Matsui, and Y. Sohrin (2001), Distribution of trace bioelements in the subarctic North Pacific Ocean and the Bering Sea (the R/V Hakuho Maru Cruise KH-97-2), *J. Oceanogr.*, *57*, 261–273.

Fujita, S., K. Kuma, S. Ishikawa, S. Nishimura, Y. Nakayama, S. Ushizaka, Y. Isoda, S. Otosaka, and T. Aramaki (2010), Iron distributions in the water column of the Japan Basin and Yamato Basin (Japan Sea), *J. Geophys. Res.*, *115*, C12001, doi: 10.1029/2010JC006123.

Gledhill, M., P. Mccormack, S. Ussher, E. P. Achterberg, R. F. C. Mantoura, and P. J. Worsfold (2004), Production of siderophore type chelates by mixed bacterioplankton populations in nutrient enriched seawater incubations, *Mar. Chem.*, *88*, 75–83.

Gledhill, M., and K. N. Buck (2012), The organic complexation of iron in the marine environment: a review, *Front. Microbiol.*, *3*, doi: 10.3389/fmicb.2012.00069.

Granger, J., M. G. Prokopenko, D. M. Sigman, C. W. Mordy, Z. M. Morse, L. V. Morales, R. N. Sambrotto, and B. Plessen (2011), Coupled nitrification-denitrification in sediment of the eastern Bering Sea shelf leads to ^{15}N enrichment of fixed N in shelf waters, *J. Geophys. Res.*, *116*, C11006, doi: 10.1029/2010JC006751.

Gruber, N., and J. L. Sarmiento (1997), Global patterns of marine nitrogen fixation and denitrification, *Global Biogeochem. Cycles*, *11*, 235–266.

Hansen, H. P. (1999), Determination of oxygen, in Methods of Seawater Analysis, edited by K. Grasshoff, K. Kremling and M. Ehrhardt, pp. 75–89, Wiley-VCH, New York.

Hassler, C. S., Alasonati, E., Nichols, C. A. M., and V. I. Slaveykova (2011a), Exopolysaccharides produced by bacteria isolated from the pelagic Southern Ocean—Role in Fe binding , chemical reactivity, and bioavailability, *Mar. Chem.*, *123*, 88–98.

Hassler, C. S., V. Schoemann, C. M. Nichols, E. C. V. Butler, and P. W. Boyd (2011b), Saccharides enhance iron bioavailability to Southern Ocean phytoplankton. *Proc. Natl. Acad. Sci. U. S. A.*, *108*, 1076–1081.

Hayase, K., and N. Shinozuka (1995), Vertical distribution of fluorescent organic matter along with AOU and nutrients in the equatorial Central Pacific, *Mar. Chem.*, *48*, 283–290.

Hayase, K., H. Tsubota, I. Sunada, S. Goda, and H. Yamazaki (1988), Vertical distribution of fluorescent organic matter in the North Pacific, *Mar. Chem.*, *25*, 373–381.

Heller, M. I., D. M. Gaiero, and P. L. Croot (2012), Basin scale survey of marine humic fluorescence in the Atlantic: Relationship to iron solubility and H_2O_2, *Global Biogeochem. Cycles*, *2013*, doi: 10.1029/2012GB004427, in press.

Hirota, A., A. Ijiri, D. D. Komatsu, S. B. Ohkubo, F. Nakagawa, and U. Tsunogai (2009), Enrichment of nitrous oxide in the water columns in the area of the Bering and Chukchi Seas, *Mar. Chem.*, *116*, 47–53.

Hurst, M. P., A. M. Aguilar-Islas, and K. W. Bruland (2010), Iron in the southeastern Bering Sea: Elevated leachable particulate Fe in shelf bottom waters as an important source for surface waters, *Cont. Shelf Res.*, *30*, 467–480.

Johnson, K. S. (2007), Developing standards for dissolved iron in seawater, *EOS Trans, AGU*, *88(*11*)*, 131–132.

Johnson, K. S., F. P. Chavez, and G. E. Friederich (1999), Continental-shelf sediment as a primary source of iron for coastal phytoplankton, *Nature*, *398*, 697–700.

Johnson, K. S., R. M. Gordon, and K. H. Coale (1997a), What controls dissolved iron concentrations in the world ocean? *Mar. Chem.*, *57*, 137–161.

Johnson, K. S., R. M. Gordon, and K. H. Coale (1997b), What controls dissolved iron concentrations in the world ocean? Authors' closing comments, *Mar. Chem.*, *57*, 181–186.

Kitayama, S., et al. (2009), Controls on iron distributions in the deep water column of the North Pacific Ocean: Iron(III) hydroxide solubility and marine humic-type dissolved organic matter, *J. Geophys. Res.*, *114*, C08019, doi: 10.1029/2008JC004754.

Kuma, K., J. Nishioka, and K. Matsunaga (1996), Controls on iron(III) hydroxide solubility in seawater: the influence of pH and natural organic chelators, *Limnol. Oceanogr.*, *41*, 396–407.

Kuma, K., A. Katsumoto, H. Kawakami, F. Takatori, and K. Matsunaga (1998). Spatial variability of Fe(III) hydroxide solubility in the water column of the northern North Pacific Ocean, *Deep-Sea Res. I*, *43*, 91–113.

Kuma, K., Y. Isoda, and S. Nakabayashi (2003), Control on dissolved iron concentrations in deep waters in the western North Pacific: Iron (III) hydroxide solubility, *J. Geophys. Res.*, *108(*C9*)*, 3289, doi: 10.1029/2002JC001481.

Laglera, L. M., and C. M. G. van den Berg (2009), Evidence for geochemical control of iron by humic substances in seawater, *Limnol. Oceanogr.*, *54*, 610–619.

Lam, P. J., and J. K. B. Bishop (2008), The continental margin is a key source of iron to the HNLC North Pacific Ocean, *Geophys. Res. Lett.*, *35*, L07608, doi: 10.1029/2008GL033294.

Lawaetz, A. J., and C. A. Stedmon (2009), Fluorescence intensity calibration using the Raman scatter peak of water, *Appl. Spectrosc.*, *63*, 936–940.

Lehmann, M. F., D. M. Sigman, D. C. McCorkle, B. G. Brunelle, S. Hoffman, M. Kienast, G. Cane, and J. Clement (2005), Origin of the deep Bering Sea nitrate deficit: Constraints from the nitrogen and oxygen isotope composition of water column nitrate and benthic nitrate fluxes, *Global Biogeochem. Cycles*, *19*, GB4005, doi: 10.1029/2005GB002508.

Luchin, V. A., V. A. Menovshchikov, V. M. Lavrentiev, and R. K. Reed (1999), Thermohaline structure and water masses in the Bering Sea, in Dynamics of the Bering Sea, edited by T. R. Loughlin and K. Ohtani, pp. 61–91, University of Alaska Sea Grant, Fairbanks, Alaska.

Martin, J. H., R. M. Gordon, S. Fitzwater, and W. W. Broenkow (1989), VERTEX: Phytoplankton/iron studies in the Gulf of Alaska, *Deep-Sea Res.*, *36*, 649–680.

Mawji, E., M. Gledhill, J. A. Milton, M. V. Zubkov, A. Thompson, G. A. Wolff, and E. P. Achterberg (2011), Production of siderophore type chelates in Atlantic Ocean waters enriched with different carbon and nitrogen sources. *Mar. Chem.*, *124*, 90–99.

Measures, C. I., M. T. Brown, and S. Vink (2005), Dust deposition to the surface waters of the western and central North Pacific inferred from surface water dissolved aluminum concentrations, *Geochem. Geophys. Geosys.*, *6*, Q09M03, doi: 10.1029/2005GC000922.

Miura, T., T. Suga and K. Hanawa (2002), Winter mixed layer and formation of dichothermal water in the Bering Sea, *J. Oceanogr.*, *58*, 815–823.

Mizobata, K., J. Wang, and S. Saitoh (2006), Eddy-induced cross-slope exchange maintaining summer high productivity of the Bering Sea shelf break, *J. Geophys. Res.*, *111*, C10017, doi: 10.1029/2005JC003335.

Mopper, K., and C. A. Schultz (1993), Fluorescence as a possible tool for studying the nature and water column distribution of DOC components, *Mar. Chem.*, *41*, 229–238.

Mordy, C. W., L. B. Eisner, P. Proctor, P. Stabeno, A. H. Devol, D. H. Shull, J. M. Napp, and T. Whiteledge (2010), Temporary uncoupling of the marine nitrogen cycle: Accumulation of nitrite on the Bering Sea shelf, *Mar. Chem.*, *121*, 157–166.

Murphy, K. R., C. A. Stedmon, T. D. Waite, and G. M. Ruiz (2008), Distinguishing between terrestrial and autochthonous organic matter sources in marine environments using fluorescence spectroscopy, *Mar. Chem.*, *108*, 40–58.

Nakabayashi, S., M. Kusakabe, K. Kuma, and I. Kudo (2001), Vertical distributions of iron(III) hydroxide solubility and dissolved iron in the northwestern North Pacific Ocean, *Geophys. Res. Lett.*, *28*, 4611–4614.

Nakabayashi, S., K. Sasaoka, S. Saitoh, M. Mochizuki, N. Shiga, and M. Kusakabe (2002), Variation in iron(III) solubility and iron concentration in the northwestern North Pacific Ocean, *Limnol. Oceanogr.*, *47*, 885–892.

Nakayama, Y., S. Fujita, K. Kuma, and K. Shimada (2011), Iron and humic-type fluorescent dissolved organic matter in the Chukchi Sea and Canada Basin of the western Arctic Ocean, *J. Geophys. Res.*, *116*, C07031, doi: 10.1029/2010JC006779.

Nishimura, S., K. Kuma, S. Ishikawa, A. Omata, and S. Saitoh (2012), Iron, nutrients, humic-type fluorescent dissolved organic matter in the northern Bering Sea shelf, Bering Strait, and Chukchi Sea, *J. Geophys. Res.*, *117*, C02025, doi: 10.1029/2011JC007355.

Nishioka, J., S. Takeda, C. S. Wang, W. K. Johnson (2001), Size-fractionated iron concentrations in the northeast Pacific Ocean: Distribution of soluble and small colloidal iron, *Mar. Chem.*, *74*, 157–179.

Nishioka, J., S. Takeda, I. Kudo, D. Tsumune, T. Yoshimura, K. Kuma, and A. Tsuda (2003), Size-fractionated iron distributions and iron-limitation processes in the subarctic NW Pacific, *Geophys. Res. Lett.*, *30(*14*)*, 1730, doi: 10.1029/2002GL016853.

Nishioka, J., S. Takeda, H. J. W. de Baar, P. L. Croot, M. Boye, P. Laan, and K. R. Timmermans (2005), Changes in the concentration of iron in different size fractions during an iron enrichment experiment in the open Southern Ocean, *Mar. Chem.*, *95*, 51–63.

Nishioka, J., et al. (2007), Iron supply to the western subarctic Pacific: Importance of iron export from the Sea of Okhotsk, *J. Geophys. Res.*, *112*, C10012, doi: 10.1029/2006JC004055.

Obata, H., H. Karatani, and E. Nakayama (1993), Automated determination of iron in seawater by chelating resin concentration and chemiluminescence detection, *Anal. Chem.*, *65*, 1524–1528.

Odate, T. (1996), Abundance and size composition of the summer phytoplankton communities in the western North Pacific Ocean, the Bering Sea , and the Gulf of Alaska, *J. Oceanogr.*, *52*, 335–351.

Parsons, T. R., Y. Maita, and C. M. Lalli (1984), A Manual of Chemical and Biological Methods for Seawater Analysis. Pergamon Press, New York.

Reed, R. K., and P. J. Stabeno (1990), Flow trajectories in the Bering Sea: Evidence for chaos. *Geophys. Res. Lett.*, *17*, 2141–2144.

Reed, R. K., G. V. Khen, P. J. Stabeno, and A. V. Verkhunov (1993), Water properties and flow over the deep Bering Sea basin, summer 1991, *Deep-Sea Res. I*, *40*, 2325–2334.

Reed, R. K., and P. J. Stabeno (1999), The Aleutian North Slope Current, in Dynamics of the Bering Sea, edited by T. R. Loughlin and K. Ohtani, pp. 177–191, University of Alaska Sea Grant, Fairbanks, Alaska.

Redfield, A. C., B. H. Ketchum, and F. A. Richards (1963), The influence of organisms on the composition of seawater, in The Sea, vol. 2, edited by M. N. Hill, pp. 26–77, Wiley Interscience, New York.

Roden, G. I. (1995), Aluetian Basin of the Bering Sea: Termohaline. Oxygen, nutrient and current structure in July 1993, *J. Geophys. Res.*, *100*, 13,539–13,554.

Roden, G. I. (2000), Flow and water property structures between the Bering Sea and Fiji in the summer of 1993, *J. Geophys. Res.*, *105*, C12, 28,595–28,612.

Rue, E. L., and K. W. Bruland (1995), Complexation of iron(III) by natural organic ligands in the central North Pacific as determined by a new competitive ligand equilibration adsorptive cathodic stripping voltammetric method. *Mar. Chem.*, *50*, 117–138.

Saino, T., K. Miyata, and A. Hattori (1979), Primary productivity in the Bering and Chukchi seas and in the northern North Pacific in 1978 summers, *Bill. Plankton Soc. Jpn.*, *26*, 96–103.

Schlosser, C., and P. L. Croot (2009), Controls on seawater Fe(III) solubility in the Mauritanian upwelling zone, *Geophys. Res. Lett.*, *36*, L18606, doi: 10.1029/2009GL038963.

Schlosser, C., C. L. De La Rocha, P. Streu, and P. L. Croot (2012), Solubility of iron in the Southern Ocean. *Limnol. Oceanogr.*, *57*, 684–697.

Shiomoto, A., S. Saitoh, K. Imai, M. Toratani, Y. Ishida, and K. Sasaoka (2002), Interannual variation in phytoplankton biomass in the Bering Sea basin in the 1990s, *Prog. Oceanogr.*, *55*, 147–163.

Stabeno, P. J., and R. K. Reed (1994), Circulation in the Bering Sea basin by satellite tracked drifters. *J. Phys. Oceanogr.*, *24*, 848–854.

Stabeno, P. J., J. D. Schumacher, and K. Ohtani (1999), The physical oceanography of the Bering Sea, in Dynamics of the Bering Sea, edited by T. R. Loughlin and K. Ohtani, pp. 1–28, University of Alaska Sea Grant, Fairbanks, Alaska.

Suzuki, R., and T. Ishimaru (1990), An improved method for the determination of phytoplankton chlorophyll using N,N-dimethylformamide, *J. Oceanogr.*, *46*, 190–194.

Takahashi, K., N. Fujita, M. Yanada, and Y. Maita (2000), Long-term biogenic particle fluxes in the Bering Sea and the central subarctic Pacific Ocean, 1990–1995, *Deep-Sea Res. I*, *47*, 1723–1759.

Takahashi, K., N. Fujitani, and M. Yanada (2002), Long term monitoring of particle fluxes in the Bering Sea and the central subarctic Pacific Ocean, 1990–2000, *Pro. Oceanogr.*, *55*, 95–112.

Takata, H., et al. (2004), Spatial variability of iron in the surface water of the northwestern North Pacific Ocean, *Mar. Chem.*, *86*, 139–157.

Takata, H., K. Kuma, S. Iwade, Y. Isoda, H. Kuroda, and T. Senjyu (2005), Comparative vertical distributions of iron in the Japan Sea, the Bering Sea and the western North Pacific Ocean, *J. Geophys. Res.*, *110*, C07004, doi: 10.1029/2004J002783.

Takata, H., K. Kuma, Y. Saitoh, M. Chikira, S. Saitoh, Y. Isoda, S. Takagi, and K. Sakaoka (2006), Comparing the vertical distribution of iron in the eastern and western North Pacific Ocean, *Geophys. Res. Lett.*, *33*, L02613, doi: 10.1029/2005GL024538.

Takata, H., K. Kuma, Y. Isoda, S. Otosaka, T. Senjyu, and M. Minagawa (2008), Iron in the Japan Sea and its implications for the physical processes in deep water, *Geophys. Res. Lett.*, *35*, L02606, doi: 10.1029/2007GL031794.

Takeda, S. (2011), Iron and phytoplankton growth in the subarctic North Pacific, *Aqua-BioSci. Monogr.*, *41*, 41–93.

Tanaka, T., I. Yasuda, K. Kuma, and J. Nishioka (2012), Vertical turbulent iron flux sustains the Green Belt along the shelf break in the southeastern Bering Sea. *Geophys. Res. Lett.*, *39*, L08603, doi: 10.1029/2012GL051164.

Tani, H., J. Nishioka, K. Kuma, H. Takata, Y. Yamashita, E. Tanoue, and T. Midorikawa (2003), Iron(III) hydroxide solubility and humic-type fluorescent organic matter in the deep water column of the Okhotsk Sea and the northwestern North Pacific Ocean, *Deep-Sea Res. I*, *50*, 1063–1078.

Tsunogai, S., M. Kusakabe, H. Iizumi, I. Koike, and A. Hattori (1979), Hydrographic features of the deep water of the Bering Sea, the sea of silica, *Deep-Sea Res., Part A*, *26*, 641–659.

Velasquez, I., B. L. Nunn, E. Ibisanmi, D. R. Goodlet, K. A. Hunter, and S. G. Sander (2011), Detection of hydroxamate siderophores in coastal and sub-Atlantic waters off the South Eastern coast of New Zealand, *Mar. Chem.*, *126*, 97–107.

Yamashita, Y., R. M. Cory, J. Nishioka, K. Kuma, E. Tanoue, and R. Jaffe (2010), Fluorescence characteristics of dissolved organic matter in the deep waters of the Okhotsk Sea and the northwestern North Pacific Ocean, *Deep-Sea Res. II*, *57*, 1478–1485.

Yoshikawa, C., T. Nakatsuka, and M. Wakatsuchi (2006), Distribution of N* in the Sea of Okhotsk and its use as a biogeochemical tracer of the Okhotsk Sea Intermediate Water formation process, *J. Mar. Sys.*, *63*, 49–62.